Ecological Modelling 410 (2019) 108777

Contents lists available at ScienceDirect

Ecological Modelling

journal homepage: www.elsevier.com/locate/ecolmodel

A highly invasive chimeric ranavirus can decimate tadpole populations rapidly through multiple transmission pathways

Angela Peace[a,b,*], Suzanne M. O'Regan[c,b], Jennifer A. Spatz[d], Patrick N. Reilly[e], Rachel D. Hill[d], E. Davis Carter[d], Rebecca P. Wilkes[e,f], Thomas B. Waltzek[g], Debra L. Miller[d,e], Matthew J. Gray[d]

[a] Department of Mathematics and Statistics, Texas Tech University, Lubbock, TX, USA
[b] National Institute for Mathematical and Biological Synthesis, University of Tennessee, Knoxville, TN, USA
[c] Department of Mathematics, North Carolina A&T State University, Greensboro, NC, USA
[d] Center for Wildlife Health, Department of Forestry, Wildlife and Fisheries, University of Tennessee Institute of Agriculture, Knoxville, TN, USA
[e] College of Veterinary Medicine, University of Tennessee, Knoxville, TN, USA
[f] Animal Disease Diagnostic Laboratory, Purdue University, West Lafayette, IN, USA
[g] Department of Infectious Diseases and Immunology, College of Veterinary Medicine, Gainesville, FL, USA

ARTICLE INFO

Keywords:
Ranavirus
Transmission
Amphibians
Disease
Model
Amphibian declines
Emerging infectious disease
Pathogen model

ABSTRACT

A consequence of genetic recombination can be the evolution of highly virulent pathogen strains. Virulence can manifest through various mechanisms of host–pathogen interaction that facilitate transmission. We discovered a highly virulent chimeric ranavirus in Georgia, USA, estimated transmission parameters using controlled experiments, and developed compartmental disease models to examine potential consequences on tadpoles of a susceptible host species (*Lithobates sylvaticus*). Our models included three transmission pathways: direct transmission via host contact, environmental transmission via shed virions in water, and transmission via necrophagy of morbid individuals. Unlike previous models, we categorized individuals into multiple stages of infection (susceptible, latency, and infectious), where the probability of disease-induced mortality increased throughout the duration of infection following a gamma distribution with an integer shape parameter. Our simulations showed that accounting for pathogen incubation improved model predictions when compared to survival data from controlled experiments. We found that transmission due to direct contact of tadpoles was the dominant transmission pathway; however, environmental transmission played a larger role as tadpole density increased and the epidemic progressed. Estimated $\mathcal{R}_0$ (basic reproduction number) values > 570 for all transmission pathways indicate that targeting only one transmission pathway is unlikely to thwart invasion. Additionally, the high invasion potential and diseased-induced mortality associated with this chimeric ranavirus indicate that this pathogen is a substantial threat to amphibian biodiversity in the United States.

1. Introduction

Identifying the importance of transmission pathways under varying conditions is fundamental to characterizing the epidemiology of host–pathogen systems (Tien and Earn, 2010). Pathogens can infect hosts through various pathways. Environmental transmission can occur through air, water or soil, and depends on various factors such as host shedding rates of the pathogen and pathogen persistence outside the host (Nelson et al., 2009; Briggs et al., 2010). Transmission can also occur through direct contact between infected and uninfected individuals, and that probability can change as disease progresses in the host (McCallum et al., 2001). If key transmission pathways can be identified, disease management or intervention strategies can be conceived to thwart or prevent an outbreak (Langwig et al., 2015).

Compartmental models, such as Susceptible-Infectious (SI) and Susceptible-Infectious-Recovered (SIR), are commonly used to characterize the epidemiology of host–pathogen systems, estimate the invasion potential of a pathogen (i.e., basic reproduction number, $\mathcal{R}_0$), and estimate outbreak size in hosts (Keeling and Rohani, 2011). These models commonly assume that the duration of host infectiousness follows an exponential distribution (Keeling and Rohani, 2011), which often is unrealistic, because this assumes that the probability of remaining infectious over time drops dramatically. More typically, duration of host infectiousness is gamma-distributed (Wearing et al., 2005; Lloyd, 2001), and consequently, individuals contribute to pathogen transmission over time frames that are closer to the mean

* Corresponding author at: Department of Mathematics and Statistics, Texas Tech University, Lubbock, TX, USA.
E-mail address: a.peace@ttu.edu (A. Peace).

https://doi.org/10.1016/j.ecolmodel.2019.108777
Received 26 March 2019; Received in revised form 12 June 2019; Accepted 29 July 2019

duration of infectiousness. Moreover, hosts that are more diseased can be more infectious. Previous investigations have expanded the infectious compartment into multiple stages, each with exponentially distributed durations, which sum together in order to approximate gamma-distributed durations of infection (Lloyd, 2001; Krylova and Earn, 2013; Wearing et al., 2005). However, few have used empirical data to estimate changes in host infectiousness through the course of disease progression. Finally, few mathematical models have explicitly incorporated heterogeneities in host infectiousness with environmental transmission, which could increase during an outbreak, especially in aquatic ecosystems where pathogens might accumulate in water.

Ranaviruses are globally emerging pathogens that affect amphibians, reptiles and fish (Gray and Chinchar, 2015). This pathogen is a double-stranded DNA virus that can infect hosts through the water or by direct contact (Brunner et al., 2007). Only one study has previously developed a compartmental (SI) model for ranaviruses, and it did not consider changes in transmission with disease progression (Duffus, 2012). That study predicted a stable equilibrium between common frog (*Rana temporaria*) adults and ranavirus in the United Kingdom (Duffus, 2012). However, the susceptibility of most adult amphibians to ranavirus is less than tadpoles, because of a more robust and rapid immune response (Grayfer et al., 2015). Indeed, catastrophic die-offs of larval wood frogs (*Lithobates sylvaticus*) involving thousands of individuals have been reported (Harp and Petranka, 2006; Brunner et al., 2011; Wheelwright et al., 2014). Population projection models suggest that ranaviruses can cause amphibian population declines and extinction (Earl and Gray, 2014; Earl et al., 2016) but those models cannot determine influential pathways.

In this study, we used a system of ordinary differential equations and empirical data to characterize the epidemiology of a recently discovered chimeric *Frog virus 3* (FV3)-like ranavirus (Claytor et al., 2017), and its potential effects on a population of wood frog tadpoles. Using our experimental results for model parameterization, we expanded previous modeling efforts (Duffus, 2012; Greer et al., 2008) to include multiple transmission pathways (i.e., direct contact, necrophagy, and environmental), stage-dependent transmission, and $\mathcal{R}_0$ estimates for each pathway. We show that incorporating multiple host infection stages for direct transmission and pathogen shedding improves model fit, and that all transmission pathways have high invasion potential, illustrating the threat of this chimeric ranavirus to biodiversity in North America.

2. Methods

2.1. Empirical methods

We performed all experiments in a controlled laboratory environment at the Johnson Animal Research and Teaching Unit of the University of Tennessee Institute of Agriculture. We collected egg masses from breeding wood frogs (*L. sylvaticus*) in the wild and reared them outdoors in wading pools until the experiments began (Tennessee Scientific Collection Permit 1990). All experiments were performed at room temperature (22–24 °C) and started when tadpoles were approximately Gosner stage 30, which is the midpoint of pre-metamorphic development for tadpoles (Wells, 2007). Water temperature and development stage are known to influence susceptibility results (Haislip et al., 2011; Brand et al., 2016), hence they were held constant in our experiments. We fed tadpoles commercial fish pellets ad libitum until the experiments began then switched to a diet of 12% of their body mass during the experiment (Hoverman et al., 2011). All experiments followed approved University of Tennessee IACUC protocol 2140.

2.1.1. Contact rate and probability of transmission given contact experiments

We estimated contact rates for wood frog tadpoles in 12-L plastic tubs (724 cm^2) that contained 5.5 L of water and 11 tadpoles, which is approximately 153 tadpoles per m^2. This is a moderate density of wood frog tadpoles based on estimates in vernal pools in North Carolina, USA (Petranka et al., 2003; Harp and Petranka, 2006). Because infection by a pathogen can change activity (Parris et al., 2005), we infected one tadpole and measured number of contacts with that tadpole during three 10-min intervals at 2, 4 and 6 h following the start of co-habitation. The tadpole was infected via a 3-day exposure in a 1 L tub to 10^3 plaque forming units (PFUs) per mL of a *Frog virus 3* (FV3)-like ranavirus (Miller et al., 2007), which is sufficient to cause infection and disease in wood frog tadpoles (Hoverman et al., 2011; Warne et al., 2011). We estimated contact rates by observing tadpoles from a distance of 1 m so not to influence activity, and recorded number of contacts with the infected individual during the 10-min observation window. There were 20 replicate tubs and each tub was observed three times. Data were summarized as number of contacts with an infected tadpole per minute then extrapolated to daily contact rates, assuming 12 h of daily activity (Wells, 2007).

We performed a second experiment to estimate the probability of transmission given contact. Similar to the previous experiment, we infected five wood frog tadpoles by exposing them to 10^3 PFU/mL of the same FV3-like isolate. Given that the probability of transmission can change with post-exposure (PE) duration to a pathogen (Lloyd, 2001), we performed direct contact exposures at 24, 48, 72 and 96 h PE. We emulated direct contact by touching each infected tadpole to five uninfected tadpoles for < 1 s then placed the animals in individual 1-L tubs and followed their fate for 14 days (Brunner et al., 2007). For consistency, the original five infected tadpoles were used for each direct contact exposure, with $n = 25$ (5 infected × 5 uninfected tadpoles) possible transmission events per 24-h time step. We humanely euthanized surviving individuals using benzocaine hydrochloride, collected a homogenate of liver and kidney tissue for virus testing (discussed later), and froze samples at −80 °C until processing. We summarized the transmission data as survival curves, because all cases of infection (as determined by quantitative polymerase chain reaction, qPCR) resulted in mortality.

2.1.2. Estimation of virus shedding rate experiment

Similar to the probability of transmission via direct contact, it is likely that pathogen shedding increases as infection progresses and becomes systemic. Hence, we estimated the daily shedding rate for wood frog tadpoles by measuring virions shed at 72, 96 and 120 h PE. As before, tadpoles ($n = 5$ per PE duration) were exposed individually to 10^3 PFU per mL of the same FV3-like isolate to initiate infection. At 72 h, all tadpoles were put into new containers with 1 L of fresh water. At 24, 48, and 72 h thereafter, we collected 50 mL of water, filtered it through a 0.2 μM filter (ThermoFisher cat no. 09-719C) to collect virions, and stored samples at −80 °C until qPCR processing (discussed below). Because water was not changed between collecting samples, each time period, except the first, represented an accumulation of virions from the previous time periods plus the addition of newly shed virions. The environmental persistence of ranavirus virions in aged, dechlorinated municipal water exceeds 7 days (Johnson and Brunner, 2014; Munro et al., 2016). Hence, we adjusted mean daily shedding rate (ω) for each time step as: $\omega_t - \omega_{t-1}$. We divided qPCR estimates of viral load in the water by 50 mL (i.e., volume of processed water sample) and present ω as PFUs produced per tadpole per mL per day.

2.1.3. Virus detection and quantification

To quantify the amount of virus DNA in tissue and water samples for the contact and shedding experiments, respectively, we used qPCR. We extracted genomic DNA (gDNA) from samples using a DNeasy Blood and Tissue Kit (Qiagen Inc., Valencia, CA) and quantified gDNA using Nanodrop technology. We performed real-time quantitative PCR (qPCR) targeting a highly conserved 70-bp region of the FV3 genome as described by Hoverman et al. (2010). Each reaction included 7.5 μL of

TaqMan Universal PCR Master Mix, 1 µL of both forward and reverse primers at 10 µM concentrations, 1 µL of MCP Probe, and 25 µg of DNA extracted from each sample. We added RNA/Nuclease-free water to each reaction to bring the total volume to 15 µL. We ran the samples at 50 °C for 2 min, 95 °C for 10 min and 95 °C for 15 s, and 60 °C for 1 min for 40 cycles. We used four controls for the qPCR: two negative controls (i.e., DNA grade water and tissue from a known ranavirus-negative tadpole) and two positive controls (i.e., virus and tissue from a known ranavirus-positive tadpole). We performed the qPCR for the shedding experiment using a Life Technologies ABI 7900 Fast Real-Time PCR System and for the contact experiment using an Applied Biosystems Quantstudio 6 Flex Real-Time PCR Systems. We fit standard curves with six serial dilutions (10^1–10^6 PFU/mL) of cultured virus for each qPCR run to determine virus presence and estimate viral load in each sample.

2.2. Modeling methods

We used the laboratory experiments (Section 2.1) to parameterize two mathematical models of ranavirus transmission dynamics in a single population of wood frog tadpoles (*Lithobathes sylvaticus*), which is a species that is highly susceptible to ranavirus (Hoverman et al., 2011). We developed a base model (Section 2.2.1) with a single infection stage and constant direct transmission and viral shedding rates. We subsequently expanded this model to include multiple stages of infection, and stage-specific transmission and viral shedding rates (Section 2.2.2).

2.2.1. Base model

We divided individuals into three subpopulations densities, susceptible $S(t)$, infectious $I(t)$, and dead $D(t)$ individuals per liter (L). The base model is composed of ordinary differential equations for these three subpopulations and the amount of virions $V(t)$, or virus particles, in the water column. The total population $N(t) = S(t) + I(t) + D(t)$ gives the total number of individuals per L. In order to relate the model to empirical estimates, we rescaled the population densities to be individuals per meter squared, which is typically observed and documented empirically. Following the experimental set up described in Section 2.1.1, we assumed that an average density of two individuals/L corresponds to 153 individuals/m^2. The model structure is shown in Fig. 1 and the equations are given below:

$$\frac{dS}{dt} = \underbrace{-Sg(I)}_{\text{direct transmission}} - \underbrace{\rho Sf(V)}_{\text{environmental transmission}} - \underbrace{Sh(D)}_{\text{necrophagy transmission}} \tag{1a}$$

$$\frac{dI}{dt} = \underbrace{Sg(I)}_{\text{direct transmission}} + \underbrace{\rho Sf(V)}_{\text{environmental transmission}} + \underbrace{Sh(D)}_{\text{necrophagy transmission}} - \underbrace{\mu I}_{\text{viral induced death}} \tag{1b}$$

$$\frac{dD}{dt} = \underbrace{\mu I}_{\text{viral induced death}} - \underbrace{\xi cSD}_{\text{necrophagy}} - \underbrace{\delta D}_{\text{natural decay}} \tag{1c}$$

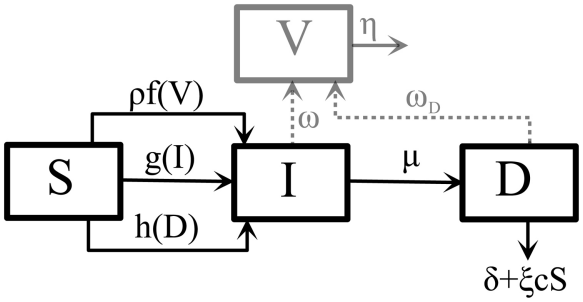

Fig. 1. Structure of the base model (1). The model tracks individuals divided into three subpopulations, susceptible $S(t)$, infected $I(t)$, and dead $D(t)$ as well as the virions in the environment $V(t)$.

$$\frac{dV}{dt} = \underbrace{\omega I + \omega_D D}_{\text{shed virions}} - \underbrace{\eta V}_{\text{degradation}} \tag{1d}$$

The base model incorporates three pathways for pathogen transmission: direct contact with infected individuals, environmental, and ingestions of dead individuals (necrophagy). Direct and necrophagy transmission are assumed to be either frequency-dependent or density-dependent. If the per-individual contact rate is assumed to be independent of population density, then transmission is frequency-dependent with rates

$$g(I) = \beta \frac{I(t)}{N(t)} \quad \text{and} \quad h(D) = \alpha \frac{D(t)}{N(t)}.$$

On the other hand, contact rates may scale linearly with population density (density-dependent transmission), i.e.,

$$g(I) = \hat{\beta} I \quad \text{and} \quad h(D) = \hat{\alpha} D(t).$$

Consequently, transmission and necrophagy coefficients are defined as

$$\hat{\beta} = \frac{\beta}{S_0}, \quad \text{and} \quad \hat{\alpha} = \frac{\alpha}{S_0}.$$

We note that defining $\hat{\beta}$ and $\hat{\alpha}$ as inversely proportional to the initial susceptible population size, $S(0) = S_0$, is an approximation for density-dependent transmission dynamics. Under these approximations, the basic reproduction number is equivalent for both types of transmission (Section 2.2.4).

Environmental transmission depends on the concentration of virus in the water as well as the successful contact rate with ranavirus virions (in plaque forming units [PFU] per mL of water) per day, ρ. The environmental transmission function takes the form of $\rho \times f(V)$, where

$$f(V) = \frac{V}{V + \kappa}$$

and κ is ranavirus ID-50 (the dose needed to infect 50% of a population). Once infected, an individual has a disease-induced mortality rate of μ. Dead individuals are assumed to persist in the environment and are depleted due to necrophagy from susceptible individuals (ξ is the proportion consumed per individual and c is the contact rate) in addition to other natural losses (δ, which incorporates natural decay and necrophagy from other species). Infected and dead individuals shed virions into the environment at rate ω and virions in the environment naturally degrade at rate η. Evidence suggests that it is extremely rare for wood frog tadpoles infected with ranavirus to recover (Hoverman et al., 2011; Warne et al., 2011), therefore, we did not include a recovered compartment in our models. We developed the models on the time scale for a single outbreak scenario and therefore do not consider any birth or natural death processes.

2.2.2. Full model

The base model (1) assumes the infectious period is exponentially-distributed; that is, the diseased induced mortality rate μ is assumed constant and does not depend on the time spent in the compartment. This assumption is epidemiologically unrealistic, as infected individuals are more likely to die as they progress through the infection (Wearing et al., 2005). Here, we update the base model so the probability of mortality increases the longer the individual resides in the infection class by using a gamma distribution with an integer shape parameter (Lloyd, 2001; Wearing et al., 2005; Krylova and Earn, 2013). Following Wearing et al. (2005), we divide the infection compartment into n subcompartments, each exponentially distributed with mean $\frac{1}{n\mu}$. The modified model can still be represented by a system of ordinary differential equations where the infection compartment is divided into n subcompartments:

$$\frac{dI_0}{dt} = S\left[\sum_{i=0}^{n} g(I_i)\right] + \rho Sf(V) + Sh(D) - n\mu I_0 \tag{2a}$$

$$\frac{dI_1}{dt} = n\mu I_0 - n\mu I_1 \tag{2b}$$

$$\vdots$$

$$\frac{dI_n}{dt} = n\mu I_{n-1} - n\mu I_n. \tag{2c}$$

The sum of a sequence of independent exponentially-distributed random variables is gamma-distributed. Here, the probability density function $p(t)$ for the full infection period is a gamma distribution with integer shape parameter n (Krylova and Earn, 2013):

$$p(t) = \frac{(n\mu)^n e^{-n\mu t} t^{n-1}}{(n-1)!}. \tag{3}$$

In this notation, $n = 1$ results in the exponentially-distributed model (1) and $n \to \infty$ results in a fixed infectious period of $\frac{1}{\mu}$ (Lloyd, 2001; Wearing et al., 2005; Krylova and Earn, 2013). We note that the probability density function $p(t)$ has mean $1/\mu$ and variance $1/(n\mu^2)$. Therefore, the full model is composed of ordinary differential equations for multiple subpopulations: susceptible $S(t)$, multiple infectious classes $I_i(t)$, $i = 0, 1, \ldots, n$, dead individuals $D(t)$, and the amount of virions $V(t)$ in the environment. The total population is $N(t) = S(t) + I_0(t) + I_1(t) + \cdots + I_n(t) + D(t)$. The model structure is shown in Fig. 2 and the equations are given below:

$$\frac{dS}{dt} = \underbrace{-S\left[\sum_{i=0}^{n} g(I_i)\right]}_{\text{direct transmission}} - \underbrace{\rho \text{Sf}(V)}_{\text{environmental transmission}} - \underbrace{\text{Sh}(D)}_{\text{necrophagy transmission}} \tag{4a}$$

$$\frac{dI_0}{dt} = \underbrace{S\left[\sum_{i=0}^{n} g(I_i)\right]}_{\text{direct transmission}} + \underbrace{\rho \text{Sf}(V)}_{\text{environmental transmission}} + \underbrace{\text{Sh}(D)}_{\text{necrophagy transmission}} - \underbrace{n\mu I_0}_{\text{infection advances}} \tag{4b}$$

$$\frac{dI_1}{dt} = \underbrace{n\mu I_0}_{\text{infection advances}} - \underbrace{n\mu I_1}_{\text{infection advances}} \tag{4c}$$

$$\vdots$$

$$\frac{dI_n}{dt} = \underbrace{n\mu I_{n-1}}_{\text{infection advances}} - \underbrace{n\mu I_n}_{\text{viral induced death}} \tag{4d}$$

$$\frac{dD}{dt} = \underbrace{n\mu I_n}_{\text{viral induced death}} - \underbrace{\xi \text{cSD}}_{\text{necrophagy}} - \underbrace{\delta D}_{\text{natural decay}} \tag{4e}$$

$$\frac{dV}{dt} = \underbrace{\sum_{i=0}^{n} \omega_i I_i + \omega_D D}_{\text{shed virions}} - \underbrace{\eta V}_{\text{degradation}} \tag{4f}$$

Model (4) incorporates multiple infection classes (I_i) with varying direct transmission rates (β_i) as well as varying viral shedding rates (ω_i). Here, the subscript i refers to the ith stage of infection. Individuals in the initial infection stages are infected but may not yet be infectious. This corresponds to a latent or incubation period (i.e., $\beta_i = 0$ for $i = 0$–2).

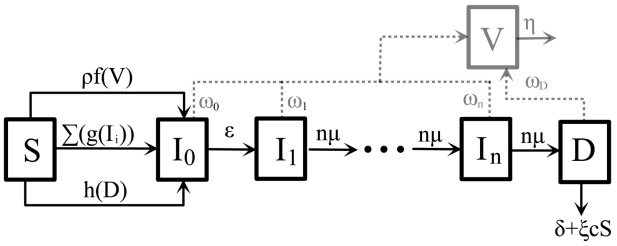

Fig. 2. Structure of the Model (4). The model tracks individuals divided into multiple subpopulations, susceptible $S(t)$, infected classes $I_i(t)$, $i = 0, 2, \ldots, n$, and dead $D(t)$ as well as the virions in the environment $V(t)$.

Furthermore, not all stages necessarily shed virus into the environment. It takes time for virions to sufficiently replicate within an infected individual (Robert et al., 2011); therefore, we assume early stages of host infection do not shed ranavirus (i.e., $\omega_i = 0$ for $i = 0$–6). Parameterization of these stages is discussed below. We assumed direct transmission to be either frequency-dependent or density-dependent.

2.2.3. Model simulations

To understand ranavirus dynamics in wood frogs, we simulated the base model (1) and the full model (4) using the parameters in Table 2 as baseline values. The rate of contact with ranavirus in water, ρ, was the only parameter that we were unable to estimate and previously published estimates do not exist. To investigate the effect of successful contact with ranavirus on disease outcomes, we varied ρ over a range of 10^2–10^6 per day.

To investigate how population density influences model dynamics, we varied the initial population size (Fig. 11), in addition to various contact rates that represent different density scenarios (Fig. 9). In order to investigate the influence of the model parameters obtained from the literature search on ranavirus dynamics, we varied environmental contact rate, virion persistence time and tadpole carcass persistence time.

2.2.4. Basic reproduction number

To elucidate the influence of each transmission pathway on invasion potential of ranavirus, we used the basic reproduction number. The basic reproduction number $\mathcal{R}_0$ is the expected number of secondary infections in a completely susceptible population produced by a single infectious individual during its infectious period (Dietz, 1993). Using model (4) we calculated the basic reproduction number of ranavirus in a population of wood frog tadpoles (A),

$$\mathcal{R}_0 = \underbrace{\frac{1}{n\mu}\sum_{i=0}^{n}\beta_i}_{\text{direct}} + \underbrace{\frac{\alpha}{\delta+\xi c}}_{\text{necrophagy}} + \underbrace{\frac{\rho S_0}{n\mu\kappa\eta(\delta+\xi c)}\left((\delta+\xi c)\sum_{i=0}^{n}\omega_i + n\mu\omega_D\right)}_{\text{environmental}} \tag{5}$$

where S_0 is the initial number of susceptible individuals. We independently examined the impact of the three transmission pathways (direct contact, environmental, and necrophagy) on ranavirus dynamics.

3. Results

3.1. Empirical results

Here, we present results of the empirical experiments and describe the parameterization of the models. All model parameters are presented in Table 2.

3.1.1. Stages of infection

To estimate the probability of remaining infectious and alive up to a specific time (i.e., the parameters in Eq. (3)), we used the probability of transmission given contact data, but restricted survival time observations to tadpoles that died and tested positive for ranavirus at the end of the 48 h, 72 h and 96 h post-exposure experiments (50 tadpoles; the 24 h PE experiment was not used because only a single infected tadpole died). We fitted the base and full models to the dead and positive data by minimizing the negative log-likelihood of each model in R (v. 3.3.1) (Table 1). Because the number of stages n must be an integer, we re-fit the full model to the data using the floor ($n = 20$) and ceiling ($n = 21$) values of n respectively (Fig. 4). Because the negative log-likelihood of the models obtained from $n = 20$, 21 respectively are equivalent to two decimal places (Table 1), we selected the $n = 20$ model (rate $n\mu = 3.927$). Since the exponential distribution is nested within the gamma distribution ($n = 1$), we used a likelihood ratio test to compare

Table 1
Comparison of models fit to the survival data obtained from the 48-h, 72-h and 96-h transmission experiments, given that tadpoles died and tested positive with ranavirus.

Candidate model	Estimated parameters	Negative log-likelihood	AIC
Exponential	$\mu = 0.201$	94.501	193.001
Gamma	$n = 20.507$, $n\mu = 4.024$	94.501	193.021
Gamma	$n = 20$, $n\mu = 3.927$	94.511	193.019
Gamma	$n = 21$, $n\mu = 4.119$	94.510	419.967

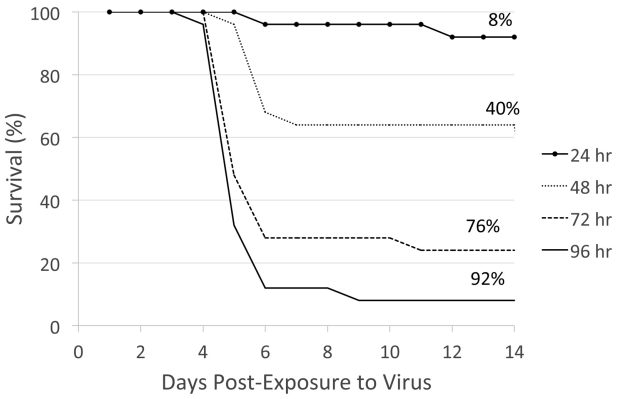

Fig. 3. Survival of wood frog (*Lithobates sylvaticus*) tadpoles that contacted an infected tadpole once 24, 48, 72, and 96 h after the infected tadpole was exposed to an infectious dose of a FV3-like ranavirus in water.

the fit of the full and base models. The base model was a poor fit to the data ($\chi^2 = 228.95$, $P < 0.0001$).

3.1.2. Direct transmission

Model (4) assumes direct transmission between an infected individual in the ith stage of infection I_i and a susceptible individual S occurs at rate β_i. Following Keeling and Rohani (2011) and Anderson and May (1992) we define β_i as a function of the successful contact rate (c) and the probability of transmission given contact (ϕ_i), where $\beta_i = -c\log(1-\phi_i)$. We estimated the average number of contacts of uninfected wood frog tadpoles with an infected tadpole to be 1.2 contacts per min (SE = 0.3), which is approximately 864 contacts per day,

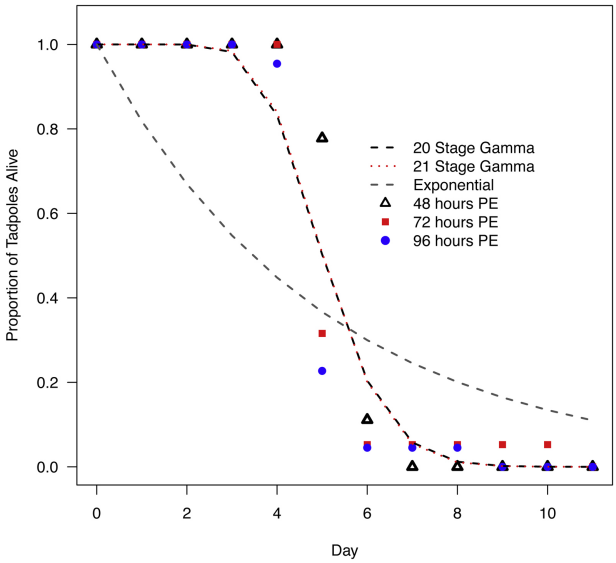

Fig. 4. Survivorship functions (Table 1) fitted to the 96-h direct contact survival curve (Fig. 3) using nonlinear least squares regression. Black triangles, red squares and blue circles are the empirical data from the direct contact experiment (Section 2.1.1) 48 h, 72 h and 96 h post-exposure to ranavirus respectively. (For interpretation of the references to color in this figure legend, the reader is referred to the web version of this article.)

assuming 12 h of activity. The probability of ranavirus transmission given contact with an infected tadpole was dependent on the stage of infection (Fig. 3). The risk of ranavirus-induced mortality due to direct contact with an infected tadpole increased on average 2.7X every 24 h, such that probability of transmission to an uninfected tadpole and subsequent mortality was 8%, 40%, 76% and 92% for 24, 48, 72 and 96 h PE to the virus, respectively. All tadpoles that died tested positive for ranavirus DNA, and those individuals that contacted infected tadpoles 72 and 96 h PE to the virus had more ranavirus in their kidney and liver tissue (Fig. 5). The empirical estimates for the probability of transmission at these given times PE were used to estimate ϕ_i for the 20 stages of infection (i = 0–19). The time spent in each infection stages comes from an exponential distribution with approximate mean of 6 h. Therefore, we assumed that $\phi_0 - \phi_2 = 0\,\%$, $\phi_3 - \phi_6 = 8\,\%$,

Table 2
Model parameters used for characterizing ranavirus transmission in a population of wood frog (*Lithobates sylvaticus*) tadpoles.

	Parameter	Values	Source
ϕ_i	Probability of infection for stages i = 0–3	0%	Survival data (Section 3.1.2)
ϕ_i	Probability of infection for stages i = 3–6	8%	Survival data (Section 3.1.2)
ϕ_i	Probability of infection for stages i = 7–10	40%	Survival data (Section 3.1.2)
ϕ_i	Probability of infection for stages i = 11–14	76%	Survival data (Section 3.1.2)
ϕ_i	Probability of infection for stages i = 15–19	92%	Survival data (Section 3.1.2)
ϕ_D	Necrophagy probability of infection	95%	Harp and Petranka (2006)
c	Contact rate	864 /day	Contact data (Section 3.1.2)
β_i	Direct transmission rate for stages i = 0–19	$\phi_i c$	Section 3.1.2
μ	Diseased induced mortality	0.1963/day	Survival data (Section 3.1.1)
ω_i	Virion shedding rate in stages i = 0–6	0 PFU/day/individual	Shedding data (Section 3.1.3)
ω_i	Virion shedding rate in stages i = 7–10	0.03 PFU/day/individual	Shedding data (Section 3.1.3)
ω_i	Virion shedding rate in stages i = 11–14	0.24 PFU/day/individual	Shedding data (Section 3.1.3)
ω_i	Virion shedding rate in stages i = 15–19	0.86 PFU/day/individual	Shedding data (Section 3.1.3)
ω_D	Dead virion shedding rate	0.86 PFU/day/individual	Shedding data (Section 3.1.3)
ρ	Successful environmental contact rate	$0–0^6$/day	Section 3.1.4
κ	ID-50	$10^{2.37}$ PFU/mL	Warne et al. (2011)
$1/\delta$	Infected carcass persistence time	2 days	Harp and Petranka (2006)
ξ	Necrophagy proportion consumed	0.057/individual	Section 3.1.4
α	Necrophagy transmission rate	$\phi_D c$	Section 3.1.4
$1/\eta$	Environmental virion persistence time	4 days	Munro et al. (2016) and Johnson and Brunner (2014)
n	Number of infection stages	20	Survival data (Section 3.1.1)

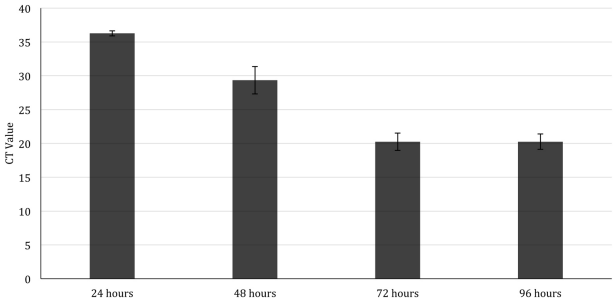

Fig. 5. Average cycle threshold (CT) value for quantitative PCR on a homogenate of kidney and liver tissue for wood frog (*Lithobates sylvaticus*) tadpoles at 24, 48, 72 and 96 h PE to the virus. CT values are equivalent to 0.07, 5.4, 1737, and 1737 virus plaque forming units per 0.25 µg of extracted gDNA, respectively.

$\phi_7 - \phi_{10} = 40\,\%$, $\phi_{11} - \phi_{14} = 76\,\%$, and $\phi_{15} - \phi_{19} = 92\,\%$. Here, the first few stages I_i for $i = 0$–2 correspond to the latent period.

3.1.3. Shedding rates

To parameterize stage-specific shedding rate ω_i for $i = 0$–19, we used the results from the shedding rate experiment (Section 2.1.2). The ability of tadpoles to shed ranavirus increased substantially with PE duration. Viral load was below detection prior to 72 h PE of hosts to the pathogen; however, the concentration of ranavirus increased on average 5X per day over the next 48 h (Fig. 6). For the first few stages of infection, we assumed $\omega_0 - \omega_6 = 0$. Given the viral loads presented in Fig. 6, we assumed $\omega_7 - \omega_{10} = .03$, $\omega_{11} - \omega_{14} = .14$, and $\omega_{15} - \omega_{19} = .86$ PFU per tadpole per day. We also assumed that infected carcasses shed virions at rates similar to the final infected stage, $\omega_D = \omega_{19}$, given that dead tadpoles are known to shed virus (Harp and Petranka, 2006).

3.1.4. Other model parameters

We obtained estimates for ID-50, survival time of ranavirus in water and mortality rate of tadpoles from necrophagy from the literature. Environmental transmission depends on the ID-50 (κ) of the host and the rate of successful host infection given contact with virions ($\rho V/(\kappa + V)$). Since κ for wood frog tadpoles has not been estimated, we used an estimate of the dose required to kill 50% of a population of wood frog tadpoles (LD-50) for our simulations (Warne et al., 2011); hence, our predictions likely are conservative. We considered the range 0–10^6/day. Munro et al. (2016) observed the length of time environmental virions persist in 30 °C water to be about five days and Johnson and Brunner (2014) observed persistence to be 3 days in 23 °C water. Therefore, we assumed virions persist four days in the environment, $\eta^{-1} = 4$ days. Finally, we assumed that necrophagy transmission is similar to direct contact. Consequently, we assumed $\alpha_i = c\phi_D$, where ϕ_D is

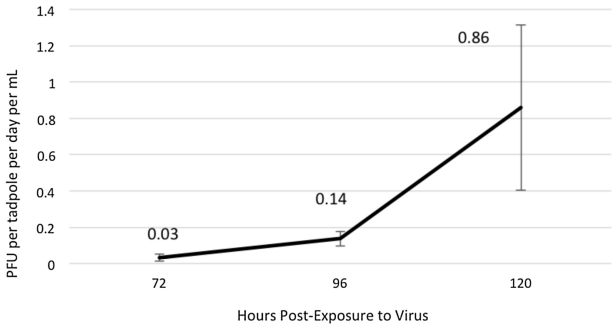

Fig. 6. Average virus produced (plaque forming units, PFU) per infected wood frog (*Lithobates sylvaticus*) tadpole per day per mL after 72, 96, and 120 h PE to the virus.

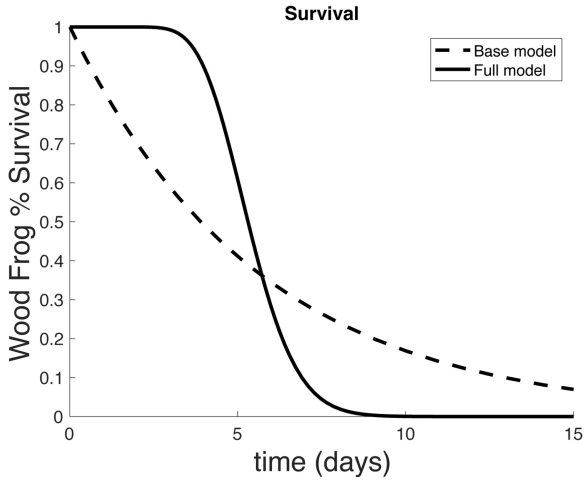

Fig. 7. Numerical simulations showing the survival percentage of the Base model (1) and Full model (4). Solid curves are the full model predictions and dashed curves are the base model predictions. Parameter values are listed in Table 1 with $\rho = 5 * 10^5$ and the base models uses $\omega = 334$ PFU/day/individual and $\phi = 86\%$. Initial conditions are an entirely susceptible initial population density $S_0 = 153/m^2$ and initial viral load of 1 PFU/mL.

the probability of transmission from consuming an infected carcass. Harp and Petranka (2006) observed nearly all infected carcasses where depleted within 48 h ($\delta^{-1} = 2$ days) and 95% of scavenging tadpoles died ($\phi_D = 95\%$). Additionally, we assumed it takes $1/\delta$ days for scavenging tadpoles to consume a carcass at contact rate c, and therefore, we parameterize the proportion consumed per individual as $\xi = \delta/c$.

3.2. Modeling results

3.2.1. Survival simulations

Both the base model (1) and the full model (4) predicted a rapid decrease in the population with populations near extinction within two weeks, but as expected from the results of the model fitting (Table 1), the full model (4) better captures the transmission dynamics (Fig. 7). The remainder of this section presents numerical simulations of the full model (4) (Figs. 8–14). In this system, both types of transmission (frequency and density dependent) cause rapid declines in amphibian

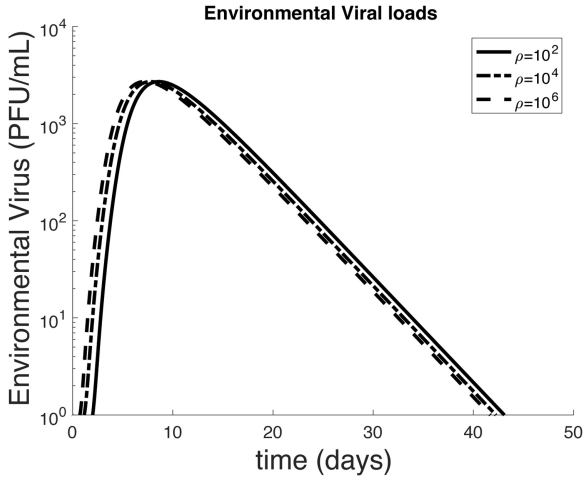

Fig. 8. Numerical simulations showing the survival percentage of Model (4) with $n = 20$ for density scenarios with varying environmental contact rates ρ. Other parameter values used are listed in Table 1. Initial conditions are an entirely susceptible initial population density $S_0 = 153/m^2$ and initial viral load of 1 PFU/mL.

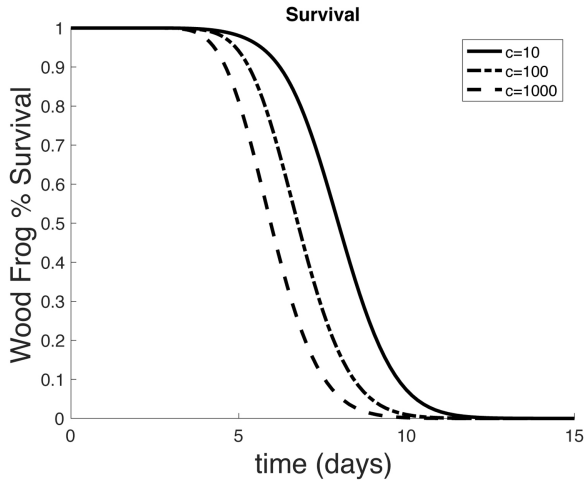

Fig. 9. Numerical simulations showing the survival percentage of Model (4) with $n = 20$ for density scenarios with varying direct contact rate, c. Other parameter values used are listed in Table 1 with $\rho = 10^4$/day. Initial conditions are an entirely susceptible initial population density $S_0 = 153/m^2$ and initial viral load of 1 PFU/mL.

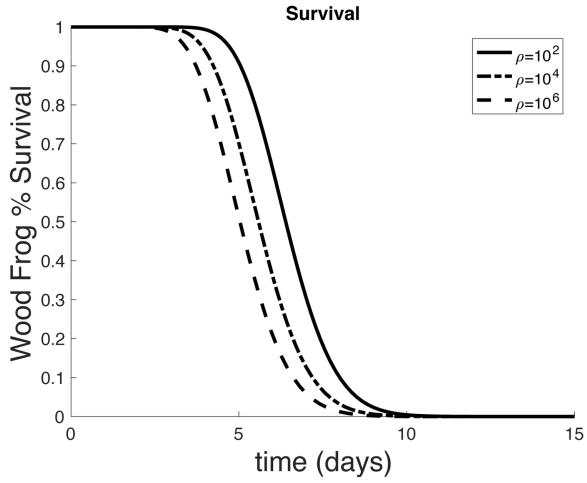

Fig. 10. Numerical simulations showing the environmental viral load of Model (4) with $n = 20$ for density scenarios with varying environmental contact rates ρ. Other parameter values used are listed in Table 1. Initial conditions are an entirely susceptible initial population density $S_0 = 153/m^2$ and initial viral load of 1 PFU/mL.

populations and the model yields similar predictions in population survival and environmental load for both scenarios. All simulations shown use frequency-dependent transmission, but the results were similar under density-dependent transmission (not shown).

Larger environmental contact rates (ρ) induce a more rapid epidemic (Fig. 8). Varying direct contact rates (c) shifted the temporal dynamics of the epidemic, with higher contact rates inducing a more rapid die-off of wood frogs (Fig. 9). Low contact rates slowed the population decline and delayed the timing of the peak in environmental viral load in water.

3.2.2. Environmental viral load simulations

The duration of ranavirus accumulation in water was robust to changes in environmental contact rate (ρ, Fig. 10). Peak environmental viral loads and ranavirus extinction time in water depended on the initial population size (Fig. 11). Peak environmental viral loads exceeded the LD-50 of $10^{2.37}$ PFU/mL (Warne et al., 2011), even for relatively low population densities (e.g., $N_0 = 77/m^2$, Fig. 11). The dynamics of the environmental viral load depended on ranavirus

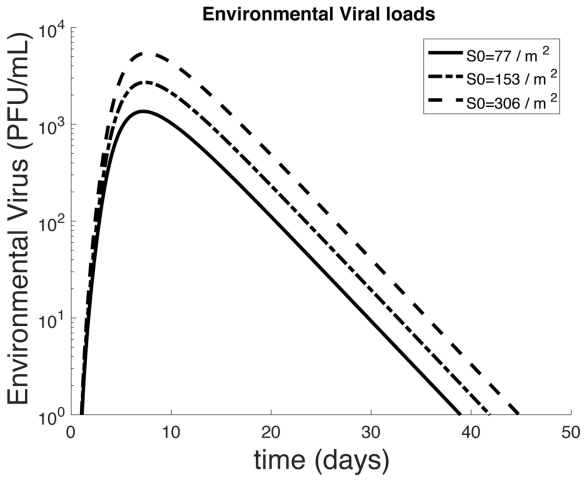

Fig. 11. Numerical simulations showing the environmental viral load in water of Model (4) with $n = 20$ for various initial population densities (S_0). Parameter values used are listed in Table 1. Initial conditions are an entirely susceptible initial population density $S_0 = 153/m^2$ and initial viral load of 1 PFU/mL.

persistence time (Fig. 12a), as well as the persistence of infected carcasses in the environment (Fig. 12b). Increasing these persistence times yielded higher environmental viral loads and increased the duration of ranavirus accumulation in water (Fig. 12).

3.2.3. Transmission pathway

All three transmission modes predicted rapid declines in the population and high environmental viral loads in water (Fig. 13). However, transmission via direct contact yielded the fastest dynamics. Epidemic take off was delayed if either environmental or necrophagy is the single mode of transmission, because it takes time for virus and infectious carcasses to accumulate in water.

All transmission pathways influenced the potential for ranavirus to invade a susceptible population of wood frog tadpoles, but this depended on population density (Table 3 and Fig. 14). The dominant pathway depended on the magnitude of the successful environmental contact rate, ρ. Direct transmission was dominant for small-medium population densities (i.e., $N_0 < 150/m^2$) for all values of ρ. Environmental transmission may become the dominant pathway for large population densities if environmental contact rate is sufficiently high (Fig. 14c); but environmental transmission pathway contributions to R_0 are not sensitive to changes in population density for moderately high environmental contact rates (e.g., $\rho = 10^4$, Fig. 14a). Direct contact transmission played a larger role than necrophagy transmission for all population densities.

4. Discussion

While any one transmission pathway on its own is influential enough to cause rapid population declines (Fig. 13), we demonstrated that transmission due to host contact is likely the most influential in low-medium population densities (Fig. 14). It is possible for environmental (waterborne) transmission to be the most influential pathway if population densities exceeds approximately 150 individuals per m^2 which is common for wood frog tadpoles (Fig. 14c). We detected virus shed by the host within 72 h PE and the rate increased nearly exponentially within 48 h (Fig. 6). The high rate of virus shedding coupled with high tadpole densities results in virus loads accumulating rapidly in the water beyond the ranavirus LD-50 ($10^{2.37}$ PFU/mL) for wood frog tadpoles (Warne et al., 2011). In addition, dead tadpoles continue to shed virus (Harp and Petranka, 2006). We assumed the environmental persistence of virions was four days, which is reasonable in pond systems (Johnson and Brunner, 2014; Munro et al., 2016). Given the duration of

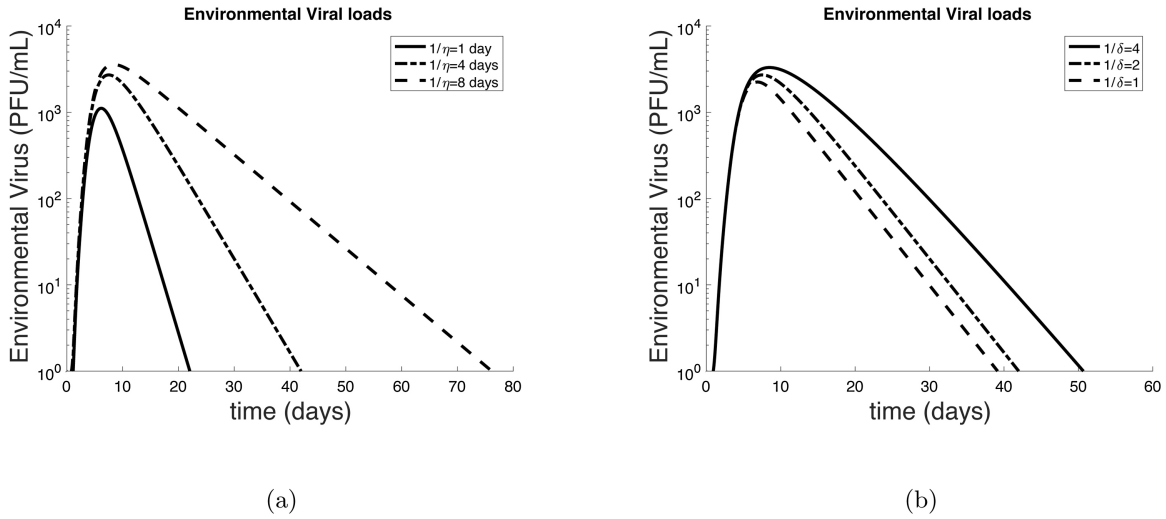

(a) (b)

Fig. 12. Numerical simulations showing the environmental viral load of the Model (4) with $n = 20$ for varying (a) environmental virion persistence time ($1/\eta$) and (b) infected carcass persistence time ($1/\delta$). Parameter values used are listed in Table 1. Initial conditions are an entirely susceptible initial population density $S_0 = 153/m^2$ and initial viral load of 1 PFU/mL.

simulated die-offs (i.e., 2 weeks) and the environmental persistence of ranavirus, our results suggest that viral loads in the water could remain above the LD-50 for wood frog tadpoles for one month and viable virions could persist for two months (Figs. 11 and 12). Environmental transmission is also a key pathway for *Batrachochytrium dendrobatidis* (*Bd*) in mountain yellow-legged frog (*Rana mucosa*) populations (Wilber et al., 2017).

Presumably, at lower densities, insufficient virus is shed by the population for environmental transmission to be most influential. At low population abundance, direct contact between tadpoles was most influential, and it was more important than the necrophagy pathway. Even at higher densities, it is likely that outbreaks are initiated through direct contact, because tadpoles do not shed virus until several days after initial infection (Fig. 6). For wood frog tadpoles, contact rates are high (ca. one per min) and likely saturate in the population even at lower densities (Brunner et al., 2017). Hence, contacts may be important to initiate ranavirus transmission, with environmental transmission becoming influential as the outbreak progresses when tadpole population densities exceeds $150/m^2$.

The lower importance of necrophagy is likely due to short persistence of dead tadpoles in the environment. Based on mesocosm research in North Carolina, USA we assumed tadpoles were eaten or decomposed within 24 h (i.e., hence available for transmission for one day, Harp and Petranka (2006)). In systems where tadpoles persist longer (e.g., northern latitudes with colder temperatures), the necrophagy pathway may play a more important role. Uninfected tadpoles that are allowed to scavenge morbid tadpoles become infected and die faster from ranaviral disease than tadpoles that are exposed to dead tadpoles but are prevented from scavenging them (Pearman et al., 2004; Harp and Petranka, 2006).

While large variations in the successful environmental contact rate (ρ) did not significantly alter model predictions of wood frog survival and environmental viral loads (Figs. 8 and 10), we found that it was an influential parameter for identifying the dominant transmission pathway (Fig. 14). Clearly, as ranavirus infects a host more efficiently through water, the environmental pathway will become more influential. Moreover, as more individuals shed virus, the environment becomes increasingly saturated with the pathogen, leading to a near-certain probability that the virus level accumulated in water results in infection of susceptible hosts. Hence, ρ can be thought of as

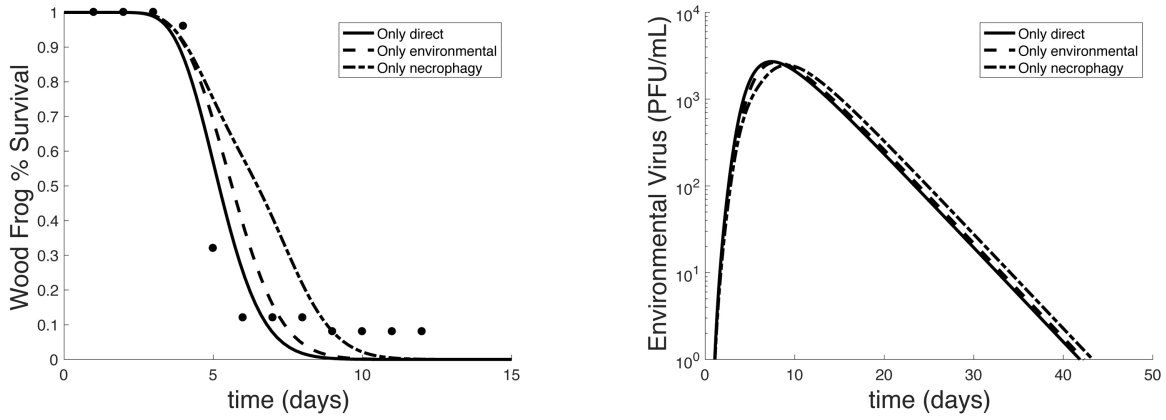

(a) Survival (b) Environmental Load

Fig. 13. Numerical simulations of Wood frog survival (a) and environmental viral load (b) of Model (4) using only a single route of transmission, either direct contact, environmental, or necrophagy. Parameter values listed in Table 1. Initial population density $S_0 = 153/m^2$ with initial conditions $S(0) = N_0 - 1$ and $I(0) = 1$. Black dots are empirical data from the direct contact experiment (Section 2.1.1) of wood frogs tadpoles exposed to the 96-h infected tadpoles.

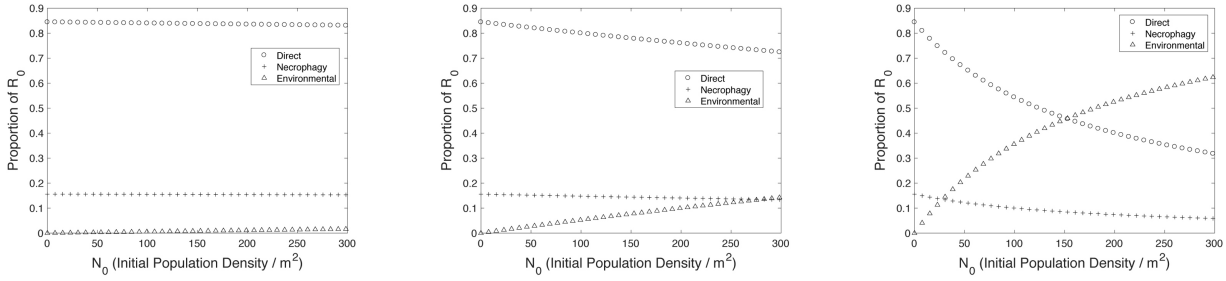

Fig. 14. Proportion of the basic reproduction number R_0 (5) from the three routes of transmission for various initial population sizes and environmental contact rates (a) $\rho = 10^4$, (b) $\rho = 10^5$, and (c) $\rho = 10^6$ per day.

Table 3
Numerical values of $\mathcal{R}_0$ given in Eq. (5) using parameter values from Table 2 and $\rho = 5 \times 10^5$.

	$N_0 = 39/m^3$	$N_0 = 153/m^3$
Direct contact transmission portion of $\mathcal{R}_0$	4557	4557
Necrophagy transmission portion of $\mathcal{R}_0$	820	820
Environmental transmission portion of $\mathcal{R}_0$	578	2268
Total $\mathcal{R}_0$	5956	7646

contributions from any factors that potentially increase the environmental transmission rate of a pathogen to a host (e.g., factors that are commonly associated with stressors or novel pathogens in naïve populations). Anthropogenic stressors, such as pesticides, have been occasionally shown to increase susceptibility to ranaviruses (Kerby and Storfer, 2009), and recent introduction of ranavirus has been one explanation for ranavirus-induced population declines in Europe (Price et al., 2014). More research is needed for robust estimates of ρ under different environmental conditions.

Our simulations predicted 100% mortality of a wood frog tadpole population in two weeks, which corresponds with the extent and rate of ranavirus outbreaks in several field reports when wood frogs are present (Greer et al., 2005; Harp and Petranka, 2006; Todd-Thompson, 2010; Brunner et al., 2011; Wheelwright et al., 2014). There are some cases, however, where ranavirus infections have been detected in wood frog populations but disease outbreaks do not occur, occur at a slower rate, or do not result in 100% mortality (Crespi et al., 2015; Hall et al., 2016), suggesting that our models do not account for all factors influencing transmission. One factor that might contribute to the simulated transmission and mortality outcomes is the FV3-like ranavirus that we used in our empirical experiments. This strain of ranavirus (RCV-Z2) was isolated from an American bullfrog (*L. catesbeianus*) farm in southern Georgia, USA (Miller et al., 2007), and it is chimeric (Claytor et al., 2017). The genome of RCV-Z2 is mostly FV3, the type species for *Ranavirus*; however, there have been at least seven recent recombination events with Common Midwife Toad Virus (CMTV, Claytor et al. (2017)), which is a strain of ranavirus that likely originated from Asia or Europe (Mavian et al., 2012). The CMTV-like ranaviruses have caused population declines of several amphibian species in Europe (Price et al., 2014) and mass die-offs of giant salamanders (*Andrias davidianus*) in China (Geng et al., 2011; Cunningham et al., 2016). The recombination events appear to be associated with immune evasion genes (Claytor et al., 2017), and have resulted in a mutated virus that is more pathogenic than native FV3-like strains in North America (Hoverman et al., 2011) and is capable of population declines (Earl and Gray, 2014; Earl et al., 2016).

There are several conditions that could have influenced our simulations. Tadpole contact rates were estimated in the laboratory with no habitat structure. Plants, detritus, and other submersed structure might change contact rates. For example, ranavirus transmission was facilitated in wetlands where cattle grazed emergent vegetation, which resulted in salamander larvae clustering and contacting each other more often (Greer et al., 2008). That said, our contact rates were similar to larger outdoor mesocosm experiments with wood frog tadpoles (Brunner et al., 2017). We also assumed that all shed virions were viable and persistence was four days. Although the environmental persistence parameters we used were estimated using pond water with microbes present (Johnson and Brunner, 2014; Munro et al., 2016), there could be other environmental factors (e.g., temperature, pH, inorganic and organic compounds) in the wild that reduce persistence. In addition, our shedding rates were estimated using qPCR, hence we do not know if all quantified virus was infectious. Although empirical experiments have demonstrated waterborne ranavirus transmission between infected and uninfected individuals without contact (Pearman et al., 2004; Brunner et al., 2007; Brenes et al., 2014), it is possible that some shed virus was not viable or inactivated faster than four days. Even so, simulated transmission dynamics indicated that ranavirus concentrations remained above the LD-50 for two weeks when virion degradation was reduced to one day (Fig. 12a). Lastly, other factors that could have influenced our simulations are life-stage and temperature dependent transmission (Hall et al., 2018). Although our simulations did not consider post-metamorphic stages, they demonstrate the potential consequences on the tadpole population, which is essential for recruitment and population persistence (Earl and Gray, 2014). Our simulations are limited to the range of temperatures (22–24 °C) that we conducted our experiments. Despite this limitation, this temperature range is experienced in many aquatic systems in North America during summer months, which corresponds when many ranavirus outbreaks are observed in the wild amphibian populations (Brunner et al., 2015; Hall et al., 2018).

To our knowledge, the $\mathcal{R}_0$ estimates from our simulations are among the highest reported for an amphibian pathogen. Estimates of $\mathcal{R}_0$ for *Bd* invasion in declining populations of mountain yellow-legged frog were 30–55 in worst-case simulation scenarios (Wilber et al., 2017). The estimates we report are similar to pathogens spread by mosquitoes at high host densities. For example, $\mathcal{R}_0$ estimates for malaria outbreaks in Africa can exceed 1000 (Davidson and Draper, 1953; Davidson, 1955; Smith et al., 2007). All simulations are estimated projections contingent upon model assumptions and the conditions for parameter estimation (Edelstein-Keshet, 2005; Allen, 2010). However, even if our estimates of $\mathcal{R}_0$ are biased by several orders of magnitude, RCV-Z2 still represents one of the most virulent pathogens reported in wildlife populations.

The site of the index case for RCV-Z2 is near Alapaha, Georgia, in the Alapaha River watershed. Wastewater from the bullfrog farm is not decontaminated; hence, the likelihood of spillover to native ectothermic vertebrate populations is high. We demonstrated that this pathogen can be transmitted to mosquitofish (*Gambusia affinis*, Brenes et al., 2014), and it is very pathogenic to multiple amphibian species, various anuran developmental stages, and for wide range of water temperatures (Hoverman et al., 2011; Haislip et al., 2011; Sutton et al.,

2014; Brand et al., 2016). As such, RCV-Z2 represents a significant conservation risk for biodiversity in North America.

Given the threat of RCV-Z2, surveillance for this pathogen should occur at a minimum in the Alapaha River watershed. In addition, it is worth considering possible disease intervention strategies given our simulations. Our results suggest that decisions should be based on population size. For small tadpole populations, efforts could be made to reduce direct contact rate, such as removal of hosts or habitat manipulations that promote dispersion of individuals (Gray et al., 2017). At high tadpole abundance, techniques should be used to reduce environmental persistence of RCV-Z2. Persistence of FV3-like ranaviruses tends to decrease as microbes in water increase (Johnson and Brunner, 2014; Munro et al., 2016). Techniques that facilitate reduction in ranavirus concentration in water could also work, such as flowing water through aquatic systems where management structures exist to manipulate hydrology (Gray et al., 2017). Mitigation strategies that target boosting host immune defenses also may be beneficial (Woodhams et al., 2011; Gray et al., 2017). However, considering that RCV-Z2 has high invasion potential for multiple transmission pathways, disease management strategies that focus on spatial containment of the pathogen (e.g., wastewater decontamination, population isolation; Gray et al. (2017) and Heard et al. (2017)) might be most effective at thwarting regional spread.

Acknowledgements

This work was supported by the USDA National Institute of Food and Agriculture, Hatch project 1012932. Part of this project was conducted while AP and SO were Postdoctoral Fellows at the National Institute for Mathematical and Biological Synthesis, an Institute sponsored by the National Science Foundation through NSF Award #DBI-1300426, with additional support from The University of Tennessee, Knoxville. We thank Bobby Simpson of the UTIA East Tennessee Research and Education Center for providing laboratory space and logistical support at the JARTU facility. We thank John Vinson for help with model fitting. We thank Jennifer Howard and Allison Graham for laboratory assistance and Linda Allen and Jesse Brunner for reviewing our models and earlier drafts of the manuscript.

Appendix A. Basic reproduction number

To obtain the basic reproduction number of ranavirus in a single-species population, $\mathcal{R}_0$, we calculate the next generation matrix with large domain (Diekmann et al., 2010). The next-generation matrix method decomposes the Jacobian matrix into two matrices that describe production of new infected cases and transitions out of infectious states respectively. The spectral radius (dominant eigenvalue) of the next-generation matrix with large domain characterizes the potential for spread of ranavirus in a naive amphibian population, and it is a critical threshold. By Theorem A.1, (Diekmann et al., 2010), the disease-free equilibrium is unstable if $\mathcal{R}_0 > 1$ and is stable if $\mathcal{R}_0 < 1$.

To obtain the basic reproduction number, we require the Jacobian matrix of system (4), which is obtained from linearizing the system. Model (4) has a line of disease-free equilibria, (S_0, 0, 0, …, 0), where $S_0 = N(0) > 0$ is the initial number of susceptibles in the population. We note that

$$g'(I_i) = \frac{\partial g(I_i)}{\partial I_i} = \begin{cases} \frac{\beta_i}{N(t)}\left(1 - \frac{I}{N(t)}\right), & \text{if transmission is frequency-dependent} \\ \hat{\beta}_i, & \text{if transmission is density-dependent.} \end{cases}$$

At a disease-free equilibrium (S_0, 0, 0, …, 0) the partial derivatives are

$$\frac{\partial g(I_i)}{\partial I_i} = \begin{cases} \frac{\beta_i}{S_0}, & \text{if transmission is frequency-dependent} \\ \hat{\beta}_i, & \text{if transmission is density-dependent.} \end{cases}$$

Note that $g'(0)S_0 = \beta_i$ for either form of transmission. Unlike density-dependent transmission, frequency dependent transmission does not depend on population density. However, it is important to note that the basic reproduction number $\mathcal{R}_0$ is defined at the beginning of an outbreak when the population density is S_0. Here, at the beginning of an outbreak, frequency and density dependent transmissions are equivalent, since the initial densities are equivalent. Additionally, we defined $\hat{\beta}$ and $\hat{\alpha}$ as inversely proportional to the initial susceptible population size, $S(0) = S_0$, as discussed in Section 2.2.1. Therefore the calculation of $\mathcal{R}_0$ should be the same for both types of transmission.

Near the disease-free equilibrium (S_0, 0, 0, …, 0), for small perturbations $\mathbf{z} = (I_0, I_1, I_2, \ldots, I_n, D, V)$ the linearized infected subsystem of (4) evolves according to the following system of equations

$$\begin{bmatrix} \dot{I}_0 \\ \dot{I}_1 \\ \dot{I}_2 \\ \vdots \\ \dot{I}_n \\ \dot{D} \\ \dot{V} \end{bmatrix} = \begin{bmatrix} -n\mu + \beta_0 & \beta_1 & \beta_2 & \ldots & \beta_{n-1} & \beta_n & \alpha & \frac{\rho S_0}{\kappa} \\ n\mu & -n\mu & 0 & \ldots & 0 & 0 & 0 & 0 \\ 0 & n\mu & -n\mu & \ldots & 0 & 0 & 0 & 0 \\ \vdots & \vdots & \vdots & \ddots & \vdots & \vdots & \vdots & \vdots \\ 0 & 0 & 0 & \ldots & n\mu & -n\mu & 0 & 0 \\ 0 & 0 & 0 & \ldots & 0 & n\mu & -\delta - \xi c & 0 \\ \omega_0 & \omega_1 & \omega_2 & \ldots & \omega_{n-1} & \omega_n & \omega_D & -\eta \end{bmatrix} \times \begin{bmatrix} I_0 \\ I_1 \\ I_2 \\ \vdots \\ I_n \\ D \\ V \end{bmatrix},$$

or equivalently,

$$\frac{d\mathbf{z}}{dt} = \mathbf{M}\mathbf{z}.$$

We decompose the matrix $\mathbf{M}$ into transmission ($\mathbf{T}$) and transition ($\mathbf{\Sigma}$) matrices respectively, obtaining

$$\frac{d\mathbf{z}}{dt} = (\mathbf{T} + \mathbf{\Sigma})\mathbf{z},$$

where

$$\mathbf{T} = \begin{bmatrix} \beta_0 & \beta_1 & \beta_2 & \dots & \beta_{n-1} & \beta_n & \alpha & \frac{\rho S_0}{\kappa} \\ 0 & 0 & 0 & \dots & 0 & 0 & 0 & 0 \\ 0 & 0 & 0 & \dots & 0 & 0 & 0 & 0 \\ \vdots & \vdots & \vdots & \ddots & \vdots & \vdots & \vdots & \vdots \\ 0 & 0 & 0 & \dots & 0 & 0 & 0 & 0 \end{bmatrix}.$$

and

$$\mathbf{\Sigma} = \begin{bmatrix} -n\mu & 0 & 0 & \dots & 0 & 0 & 0 & 0 \\ n\mu & -n\mu & 0 & \dots & 0 & 0 & 0 & 0 \\ 0 & n\mu & -n\mu & \dots & 0 & 0 & 0 & 0 \\ \vdots & \vdots & \vdots & \ddots & \vdots & \vdots & \vdots & \vdots \\ 0 & 0 & 0 & \dots & n\mu & -n\mu & 0 & 0 \\ 0 & 0 & 0 & \dots & 0 & n\mu & -\delta-\xi c & 0 \\ \omega_0 & \omega_1 & \omega_2 & \dots & \omega_{n-1} & \omega_n & \omega_D & -\eta \end{bmatrix}$$

Each entry of the transmission matrix T_{ij} denotes the rate of occurrence of new infected cases in state i arising from state j. In this model, infectious individuals in classes I_1, …, I_n, dead individuals and virions in the environment all contribute to new infections. All other non-zero transitions between states are included in the transition matrix $\mathbf{\Sigma}$, including shedding of ranavirus into the environment by infectious individuals in compartment I_n and by dead individuals.

The next-generation matrix with large domain is $\mathbf{K} = -\mathbf{T}\mathbf{\Sigma}^{-1}$. Since $\mathbf{T}$ has rank 1 (because only the first row has non-zero entries, and consequently, $\mathbf{T}$ has only one linearly independent row vector), the NGM $\mathbf{K}$ also has rank 1. Therefore, only the first row of $\mathbf{K}$ contains non-zero entries. Consequently, the spectral radius of $\mathbf{K}$ is the first entry on the diagonal,

$$K_{1,1} = \frac{1}{n\mu}\sum_{i=0}^{n}\beta_i + \frac{\alpha}{\delta+\xi c} + \frac{\rho S_0}{n\mu\kappa\eta(\delta+\xi c)}\left((\delta+\xi c)\sum_{i=0}^{n}\omega_i + n\mu\omega_D\right).$$

The entry $K_{1,1}$ is equivalent to $\mathcal{R}_0$, and it is the same for both frequency and density dependent direct transmission.

References

Allen, L.J., 2010. An Introduction to Stochastic Processes with Applications to Biology. CRC Press.

Anderson, R.M., May, R.M., 1992. Infectious Diseases of Humans: Dynamics and Control. Oxford University Press.

Brand, M.D., Hill, R.D., Brenes, R., Chaney, J.C., Wilkes, R.P., Grayfer, L., Miller, D.L., Gray, M.J., 2016. Water temperature affects susceptibility to ranavirus. EcoHealth 13 (2), 350–359.

Brenes, R., Gray, M.J., Waltzek, T.B., Wilkes, R.P., Miller, D.L., 2014. Transmission of ranavirus between ectothermic vertebrate hosts. PLOS ONE 9 (3), e92476.

Briggs, C.J., Knapp, R.A., Vredenburg, V.T., 2010. Enzootic and epizootic dynamics of the chytrid fungal pathogen of amphibians. Proc. Natl. Acad. Sci. U. S. A. 107 (21), 9695–9700.

Brunner, J., Schock, D., Collins, J., 2007. Transmission dynamics of the amphibian ranavirus *Ambystoma tigrinum* virus. Dis. Aquat. Org. 77 (2), 87–95.

Brunner, J.L., Barnett, K.E., Gosier, C.J., McNulty, S.A., Rubbo, M.J., Kolozsvary, M.B., 2011. Ranavirus infection in die-offs of vernal pool amphibians in New York, USA. Herpetol. Rev. 42 (1), 76.

Brunner, J.L., Storfer, A., Gray, M.J., Hoverman, J.T., 2015. Ranavirus Ecology and Evolution: From Epidemiology to Extinction. Springer International Publishing, Cham, pp. 71–104.

Brunner, J.L., Beaty, L., Guitard, A., Russell, D., 2017. Heterogeneities in the infection process drive ranavirus transmission. Ecology 98 (2), 576–582.

Claytor, S.C., Subramaniam, K., Landrau-Giovannetti, N., Chinchar, V.G., Gray, M.J., Miller, D.L., Mavian, C., Salemi, M., Wisely, S., Waltzek, T.B., 2017. Ranavirus phylogenomics: signatures of recombination and inversions among bullfrog ranaculture isolates. Virology 511, 330–343.

Crespi, E.J., Rissler, L.J., Mattheus, N.M., Engbrecht, K., Duncan, S.I., Seaborn, T., Hall, E.M., Peterson, J.D., Brunner, J.L., 2015. Geophysiology of wood frogs: landscape patterns of prevalence of disease and circulating hormone concentrations across the eastern range. Integr. Comp. Biol. 55 (4), 602–617.

Cunningham, A.A., Turvey, S.T., Zhou, F., Meredith, H.M., Guan, W., Liu, X., Sun, C., Wang, Z., Wu, M., 2016. Development of the Chinese giant salamander *Andrias davidianus* farming industry in Shaanxi Province, China: conservation threats and opportunities. Oryx 50 (2), 265–273.

Davidson, G., 1955. Further studies of the basic factors concerned in the transmission of malaria. Trans. R. Soc. Trop. Med. Hyg. 49 (4), 339–350.

Davidson, G., Draper, C., 1953. Field studies of some of the basic factors concerned in the transmission of malaria. Trans. R. Soc. Trop. Med. Hyg. 47 (6), 522–535.

Diekmann, O., Heesterbeek, J.A.P., Roberts, M.G., 2010. The construction of next-generation matrices for compartmental epidemic models. J. R. Soc. Interface 7 (47), 873–885.

Dietz, K., 1993. The estimation of the basic reproduction number for infectious diseases. Stat. Methods Med. Res. 2 (1), 23–41.

Duffus, A.L., 2012. Ranavirus Ecology in Common Frogs (*Rana temporaria*) from the United Kingdom: Transmission Dynamics, Alternate Hosts, and Host–Strain Interactions (University of London dissertation).

Earl, J.E., Gray, M.J., 2014. Introduction of ranavirus to isolated wood frog populations could cause local extinction. EcoHealth 11 (4), 581–592.

Earl, J.E., Chaney, J.C., Sutton, W.B., Lillard, C.E., Kouba, A.J., Langhorne, C., Krebs, J., Wilkes, R.P., Hill, R.D., Miller, D.L., et al., 2016. Ranavirus could facilitate local extinction of rare amphibian species. Oecologia 182 (2), 611–623.

Edelstein-Keshet, L., 2005. Mathematical Models in Biology. SIAM.

Geng, Y., Wang, K., Zhou, Z., Li, C., Wang, J., He, M., Yin, Z., Lai, W., 2011. First report of a ranavirus associated with morbidity and mortality in farmed Chinese giant salamanders (*Andrias davidianus*). J. Comp. Pathol. 145 (1), 95–102.

Gray, M.J., Chinchar, V.G., 2015. Introduction: history and future of ranaviruses. Ranaviruses. Springer, pp. 1–7.

Gray, M.J., Duffus, A.L., Hamam, K.H., Harris, R.N., Allender, M.C., Thompson, T.A., Christman, M.R., Sacerdote-velat, A., Sprague, L.A., Williams, J.M., et al., 2017. Pathogen surveillance in herpetofaunal populations: guidance on study design, sample collection, biosecurity, and intervention strategies. Herpetol. Rev. 48 (2), 334–351.

Grayfer, L., Edholm, E.S., Andino, F.D.J., Chinchar, V.G., Robert, J., 2015. Ranavirus host immunity and immune evasion. Ranaviruses. Springer, pp. 141–170.

Greer, A.L., Berrill, M., Wilson, P.J., 2005. Five amphibian mortality events associated with ranavirus infection in south central Ontario, Canada. Dis. Aquat. Org. 67 (1–2), 9–14.

Greer, A.L., Briggs, C.J., Collins, J.P., 2008. Testing a key assumption of host–pathogen theory: density and disease transmission. Oikos 117 (11), 1667–1673.

Haislip, N.A., Gray, M.J., Hoverman, J.T., Miller, D.L., 2011. Development and disease: how susceptibility to an emerging pathogen changes through anuran development. PLoS ONE 6 (7), e22307.

Hall, E.M., Crespi, E.J., Goldberg, C.S., Brunner, J.L., 2016. Evaluating environmental DNA-based quantification of ranavirus infection in wood frog populations. Mol. Ecol. Resour. 16 (2), 423–433.

Hall, E.M., Goldberg, C., Brunner, J., Crespi, E., 2018. Seasonal dynamics and potential drivers of ranavirus epidemics in wood frog populations. Oecologia 188 (4), 1253–1262.

Harp, E.M., Petranka, J.W., 2006. Ranavirus in wood frogs (*Rana sylvatica*): potential sources of transmission within and between ponds. J. Wildl. Dis. 42 (2), 307–318.

Heard, G.W., Scroggie, M.P., Ramsey, D.S., Clemann, N., Hodgson, J.A., Thomas, C.D., 2017. Can habitat management mitigate disease impacts on threatened amphibians? Conserv. Lett. 11 (2), e12375.

Hoverman, J.T., Gray, M.J., Miller, D.L., 2010. Anuran susceptibilities to ranaviruses: role of species identity, exposure route, and a novel virus isolate. Dis. Aquat. Org. 89 (2), 97–107.

Hoverman, J.T., Gray, M.J., Haislip, N.A., Miller, D.L., 2011. Phylogeny, life history, and ecology contribute to differences in amphibian susceptibility to ranaviruses. EcoHealth 8 (3), 301–319.

Johnson, A., Brunner, J., 2014. Persistence of an amphibian ranavirus in aquatic communities. Dis. Aquat. Org. 111 (2), 129–138.

Keeling, M.J., Rohani, P., 2011. Modeling Infectious Diseases in Humans and Animals. Princeton University Press.

Kerby, J.L., Storfer, A., 2009. Combined effects of atrazine and chlorpyrifos on susceptibility of the tiger salamander to *Ambystoma tigrinum* virus. EcoHealth 6 (1), 91–98.
Krylova, O., Earn, D.J., 2013. Effects of the infectious period distribution on predicted transitions in childhood disease dynamics. J. R. Soc. Interface 10 (84) 20130098.
Langwig, K.E., Frick, W.F., Reynolds, R., Parise, K.L., Drees, K.P., Hoyt, J.R., Cheng, T.L., Kunz, T.H., Foster, J.T., Kilpatrick, A.M., 2015. Host and pathogen ecology drive the seasonal dynamics of a fungal disease, white-nose syndrome. Proc. R. Soc. Lond. B: Biol. Sci. 282 (1799) 20142335.
Lloyd, A.L., 2001. Destabilization of epidemic models with the inclusion of realistic distributions of infectious periods. Proc. R. Soc. Lond. B: Biol. Sci. 268 (1470), 985–993.
Mavian, C., López-Bueno, A., Balseiro, A., Casais, R., Alcamí, A., Alejo, A., 2012. The genome sequence of the emerging common midwife toad virus identifies an evolutionary intermediate within ranaviruses. J. Virol JVI-07108.
McCallum, H., Barlow, N., Hone, J., 2001. How should pathogen transmission be modelled? Trends Ecol. Evol. 16 (6), 295–300.
Miller, D.L., Rajeev, S., Gray, M.J., Baldwin, C.A., 2007. Frog virus 3 infection, cultured American bullfrogs. Emerg. Infect. Dis. 13 (2), 342.
Munro, J., Bayley, A.E., McPherson, N.J., Feist, S.W., 2016. Survival of frog virus 3 in freshwater and sediment from an English lake. J. Wildl. Dis. 52 (1), 138–142.
Nelson, E.J., Harris, J.B., Morris Jr., J.G., Calderwood, S.B., Camilli, A., 2009. Cholera transmission: the host, pathogen and bacteriophage dynamic. Nat. Rev. Microbiol. 7 (10).
Parris, M.J., Storfer, A., Collins, J.P., Davidson, E.W., 2005. Life-history responses to pathogens in tiger salamander (*Ambystoma tigrinum*) larvae. J. Herpetol. 39 (3), 366–372.
Pearman, P.B., Garner, T.W., Straub, M., Greber, U.F., 2004. Response of the Italian agile frog (*Rana latastei*) to a ranavirus, frog virus 3: a model for viral emergence in naive populations. J. Wildl. Dis. 40 (4), 660–669.
Petranka, J.W., Murray, S.S., Kennedy, C.A., 2003. Responses of amphibians to restoration of a southern Appalachian wetland: perturbations confound post-restoration assessment. Wetlands 23 (2), 278–290.
Price, S.J., Garner, T.W., Nichols, R.A., Balloux, F., Ayres, C., de Alba, A.M.C., Bosch, J., 2014. Collapse of amphibian communities due to an introduced ranavirus. Curr. Biol. 24 (21), 2586–2591.
Robert, J., George, E., Andino, F.D.J., Chen, G., 2011. Waterborne infectivity of the ranavirus frog virus 3 in *Xenopus laevis*. Virology 417 (2), 410–417.
Smith, D.L., McKenzie, F.E., Snow, R.W., Hay, S.I., 2007. Revisiting the basic reproductive number for malaria and its implications for malaria control. PLoS Biol. 5 (3), e42.
Sutton, W.B., Gray, M.J., Hardman, R.H., Wilkes, R.P., Kouba, A.J., Miller, D.L., 2014. High susceptibility of the endangered dusky gopher frog to ranavirus. Dis. Aquat. Org. 112 (1), 9–16.
Tien, J.H., Earn, D.J., 2010. Multiple transmission pathways and disease dynamics in a waterborne pathogen model. Bull. Math. Biol. 72 (6), 1506–1533.
Todd-Thompson, M., 2010. Seasonality, Variation in Species Prevalence, and Localized Disease for Ranavirus in Cades Cove (Great Smoky Mountains National Park) Amphibians.
Warne, R.W., Crespi, E.J., Brunner, J.L., 2011. Escape from the pond: stress and developmental responses to ranavirus infection in wood frog tadpoles. Funct. Ecol. 25 (1), 139–146.
Wearing, H.J., Rohani, P., Keeling, M.J., 2005. Appropriate models for the management of infectious diseases. PLoS Med. 2 (7), 621.
Wells, K.D., 2007. The Ecology and Behavior of Amphibians. University of Chicago Press.
Wheelwright, N.T., Gray, M.J., Hill, R.D., Miller, D.L., 2014. Sudden mass die-off of a large population of wood frog (*Lithobates sylvaticus*) tadpoles in Maine, USA, likely due to ranavirus. Herpetol. Rev. 45 (240-L 242).
Wilber, M.Q., Knapp, R.A., Toothman, M., Briggs, C.J., 2017. Resistance, tolerance and environmental transmission dynamics determine host extinction risk in a load-dependent amphibian disease. Ecol. Lett. 20 (9), 1169–1181.
Woodhams, D.C., Bosch, J., Briggs, C.J., Cashins, S., Davis, L.R., Lauer, A., Muths, E., Puschendorf, R., Schmidt, B.R., Sheafor, B., et al., 2011. Mitigating amphibian disease: strategies to maintain wild populations and control chytridiomycosis. Front. Zool. 8 (1), 8.